PERGAMON

International Journal of Heat and Mass Transfer 44 (2001) 3765–3774

International Journal of HEAT and MASS TRANSFER

www.elsevier.com/locate/ijhmt

Three-dimensional oscillatory thermocapillary convection in liquid bridge under microgravity

Zhong Zeng [a,*], Hiroshi Mizuseki [a], Kiyoshi Simamura [a], Tsuguo Fukuda [a], Kazuyuki Higashino [b], Yoshiyuki Kawazoe [a]

[a] *Institute for Materials Research, Tohoku University, Sendai 980-8577, Japan*
[b] *Space Experiment System Development Department, IHI, Tokyo 190-1297, Japan*

Abstract

Three-dimensional oscillatory thermocapillary convection in silicone oil liquid bridge is studied numerically by means of finite volume method (FVM). The results reveal the existence of two different oscillatory modes: pulsating and rotating oscillations. Close to the onset of oscillation, the pulsating oscillatory convection is observed. With the increment of Marangoni number *Ma*, the pulsating oscillatory convection is replaced by rotating oscillatory convection, where the temperature and velocity fields demonstrate the characteristics of rotation. An approximately linear relationship between *Ma* and dimensionless main frequency $f^* = fH^2\varkappa^{-1}$ is found for $As = 4.0$ in periodic oscillatory regime. This relationship becomes a little more complex for $As = 1.0$.

Keywords: Thermocapillary; Marangoni convection; Microgravity; Instability; Floating zone; Half-zone; Liquid bridge

1. Introduction

There is a growing awareness of the significance of thermocapillary and Marangoni convection in fluid associated with gradients in surface tension to a wide variety of materials processes. The significance of the Marangoni effect in liquid metal and semiconductor processes is shown to be particularly strong and is a major factor in guiding the control of industrial processes. The floating zone technique is a promising containerless method to realize higher-quality crystals of semiconductors under microgravity. Thermocapillary convection is important for mass and heat transport in crystal growth and is investigated with half-zone liquid bridge model in the present paper.

So far, there have been some experiments both on the earth and in space to examine the thermocapillary flow in half-zone liquid bridge [1–9]. The experimental studies on the relationship between *Ma* and oscillatory main frequencies of thermocapillary flow in half-zone were conducted in [1,6,8]. The approximate linear relationship between *Ma* and oscillatory frequency for $NaNO_3$ liquid bridge with $As > 1$ was found on the earth [1]. Velten et al. [6] reported that the main trend is a slight increment of the frequency with increasing ΔT ($Ma \propto \Delta T$). The average linear dependence of frequency on ΔT is only a rough approximation. One of the typical features for zones with $As \approx 1$ is that the frequency decreases firstly then increases again at higher ΔT (larger *Ma*). Schwabe and Frank [8] presented that the oscillatory main frequency f was approximately proportional to *Ma* for $As = 1.5$, and they also reported that more typical frequency property was that: with increasing *Ma*, higher frequencies are obtained at near the onset of oscillation, then the oscillatory main frequency jumps to a lower value, and next it keeps as a constant, finally it increases with the increment of *Ma*.

Two types of oscillations were found both experimentally and numerically. Frank and Schwabe [7] reported that both pulsating and rotating oscillations were observed for azimuthal wave numbers $m = 1$ and 2 in their experiment. The numerical result of Savino and Monti [10] revealed that immediately after the onset of instability, the pulsating oscillatory flow is excited, then this pulsating oscillation mode is taken

* Corresponding author. Tel.: +81-22-215-2057; fax: +81-22-215-2052.
E-mail address: zzeng@imr.tohoku.ac.jp (Z. Zeng).

0017-9310/01/$ - see front matter
PII: S0017-9310(01)00012-6

Nomenclature

As	aspect ratio H/R
f	oscillatory frequency
f^*	dimensionless frequency $fH^2\varkappa^{-1}$
Gr	Grashof number $\alpha\Delta TgH^3/v^2$
H	height of the liquid bridge
k	thermal conductivity
Ma	Marangoni number $\sigma_k\Delta TH/(\varrho v\varkappa)$
$\mathbf{n}_\theta, \mathbf{n}_r$ and $\mathbf{n}_z$	unit vector in azimuthal, radial, and axial direction, respectively
Pr	Prandtl number $v/\varkappa$
$\mathbf{r}^*(\theta^*, r^*, z^*)$	dimensionless coordinate in circumferential, radial, and axial direction, respectively
R	radius of liquid bridge
R^*	dimensionless radius of liquid bridge
Re	thermocapillary Reynolds number
$\sigma_k\Delta TH/(\varrho v^2)$	Ma/Pr
t^*	dimensionless time $t\varkappa H^{-2}$
T	temperature
T^*	dimensionless temperature $(T-T_m)/\Delta T$
T_h	temperature at hot disc
T_c	temperature at cold disc
T_m	$(T_\mathrm{h}+T_\mathrm{c})/2$
$\mathbf{u}(u,v,w)$	velocity vector respect to $\mathbf{r}(\theta,r,z)$
$\mathbf{u}^*(u^*,v^*,w^*)$	dimensionless velocity vector
α	linear temperature expansion coefficient
δ	Kronecker operator
ΔT	temperature difference between two discs $T_\mathrm{h}-T_\mathrm{c}$
$\varkappa$	thermal diffusivity
v	kinematical viscosity
ϱ	density
σ	surface tension
σ_0	surface tension at T_m
σ_k	surface tension coefficient
∇	the gradient operator in cylindrical coordinate

over by rotating oscillation with the further increment of Ma. Yasuhiro et al. [11] also reported two types of oscillatory modes: pulsating and rotating oscillations in their 3D direct numerical simulation based on finite difference scheme. Besides, Leypoldt et al. [12] studied numerically thermocapillary convection beyond the first symmetry-breaking in both high-Pr and low-Pr liquid bridge. The composition of the supercritical flow is investigated in terms of the amplitudes of the critical mode and its higher spatial harmonics. The present paper aims to study systematically the Ma effects on oscillatory modes and frequencies in periodic oscillatory regime.

2. Mathematical models

The half-zone liquid bridge is a typical model to study thermocapillary flow in floating zone [1–13], and it is also adopted in the present study. The half-zone with a non-deformable cylindrical free surface of radius R is suspended between two discs with different temperatures as shown in Fig. 1. The temperature difference and height between two discs are ΔT and H, respectively. The liquid is assumed as a Newtonian fluid with constant kinematical viscosity and density. Liquid surface is idealized to be adiabatic from the environmental gas. A cylindrical coordinate system with its origin at the center of the bottom of liquid column is used. The surface tension is considered to be a linearly decreasing function of the temperature as $\sigma=\sigma_0-\sigma_k T$.

For incompressible fluid, the governing equations in the Boussinesq approximation are:

Continuity equation:

$$\nabla\cdot\mathbf{u}=0, \tag{1}$$

Momentum equation:

$$\varrho(\partial\mathbf{u}/\partial\mathrm{t})+\varrho(\mathbf{u}\cdot\nabla)\mathbf{u}-\varrho v\nabla^2\mathbf{u} = -\nabla P+\alpha\varrho(T_m-T)g\mathbf{n}_z+\mathbf{F}_\mathrm{s}\delta(r-R), \tag{2}$$

Energy equation:

$$\varrho C_\mathrm{p}(\partial T/\partial t)+\varrho C_\mathrm{p}(\mathbf{u}\cdot\nabla)T-k\nabla^2T=0, \tag{3}$$

where ∇ denotes the gradient operator in cylindrical coordinates; δ indicates Kronecker operator; $\mathbf{F}_\mathrm{s}\delta(r-R)$ represents surface tension $\mathbf{F}_\mathrm{s}$ which only acts on the free surface ($r=R$); α stands for linear expansion coefficient,

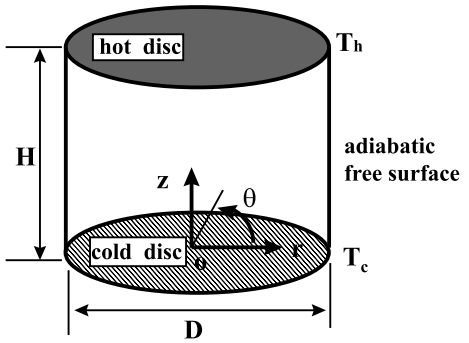

Fig. 1. Geometry and coordinate system.

$\mathbf{u}$ for velocity vector, ϱ for density, C_p for specific heat, k for thermal conductivity, g for gravity, P for pressure, v for kinematic viscosity. Surface tension on cylindrical free surface is

$$\mathbf{F}_s = (1/R)(\partial\sigma/\partial\theta)\mathbf{n}_\theta - \sigma/R\mathbf{n}_r + (\partial\sigma/\partial z)\mathbf{n}_z. \quad (4)$$

where $\mathbf{n}_\theta, \mathbf{n}_r$ and $\mathbf{n}_z$ are unit vectors in θ, r and z directions, respectively.

Due to the hypothesis of non-deformable free surface, the surface tension component in r direction loses its effect, and Eq. (4) can be simplified as

$$\mathbf{F}_s = (1/R)(\partial\sigma/\partial\theta)\mathbf{n}_\theta + (\partial\sigma/\partial z)\mathbf{n}_z. \quad (5)$$

The scales H, $H^2/\varkappa, \varkappa/H$, and $\varrho\varkappa^2/H^2$ are adopted for length, time, velocity, and pressure. Here, $\varkappa$ denotes thermal diffusivity. Scaled dimensionless temperature is $T^* = (T - T_m)/\Delta T$ with $T_m = (T_h + T_c)/2$ and $\Delta T = T_h - T_c$. The important dimensionless parameters are Prandtl number $Pr = v/\varkappa$, Grashof number $Gr = \alpha\Delta T g H^3/v^2$, aspect ratio $As = H/R$ and Marangoni number $Ma = \sigma_k \Delta T H/(\varrho v \varkappa)$.

Dimensionless basic equations take the form

$$\nabla \cdot \mathbf{u}^* = 0, \quad (6)$$

$$\partial\mathbf{u}^*/\partial t^* + (\mathbf{u}^* \cdot \nabla)\mathbf{u}^* - Pr\nabla^2\mathbf{u}^* = -\nabla P^* - GrPr^2 T^* \mathbf{n}_z - [(1/R^*)(\partial T^*/\partial\theta^*)\mathbf{n}_\theta + \partial T^*/\partial z^* \mathbf{n}_z] MaPr\delta(r^* - R^*), \quad (7)$$

$$\partial T^*/\partial t^* + (\mathbf{u}^* \cdot \nabla)T^* - \nabla^2 T^* = 0. \quad (8)$$

Boundary conditions are:

Upper-disc : non-slip and fixed temperature $T^* = 0.5$.

Lower-disc : non-slip and fixed temperature $T^* = -0.5$.

Free surface : impervious to flow of mass, momentum and energy.

For some cases, quiescent liquid with linear temperature distribution along z-axis $T^* = z^* - 0.5$ is taken as initial conditions. In order to save CPU time, the solution for similar conditions (identical Pr and As, but a little different Ma) is also used as initial condition for some cases.

By rewriting the above basic equations in the conservative form, and then integrating over a control volume, equations are discretized by finite volume method (FVM) with staggered grid. Instead of inducing surface tension in boundary conditions as the balance between shear stress and surface tension in literature [10–13], the surface tension is induced directly as the source term in momentum Eqs. (2) and (5) with δ operator. Although both boundary condition and source term can be treated as the same way in FVM, the integration form in the control volume CV for surface tension term in Eq. (2) becomes $\int_{cv} \mathbf{F}_s \delta(r - R)\,dv = \int_A \mathbf{F}_s\,ds$ (A represents area of free surface). The discretization and coding for surface tension $\int_A \mathbf{F}_s\,ds$ is straightforward in FVM. SMART (bounded QUICK) scheme is applied to convection term to solve velocity and temperature. Non-uniform grids were adopted to increase the resolution, and the local finer grids in the region near the solid discs and free surface as shown in Fig. 2 are used for the reason of the steep temperature and velocity gradients near two discs. The flow field is solved by an improved SIMPLE algorithm. The grids ($N_\theta \times N_r \times N_z$) adopted in the present computations are $40 \times 24 \times 40$

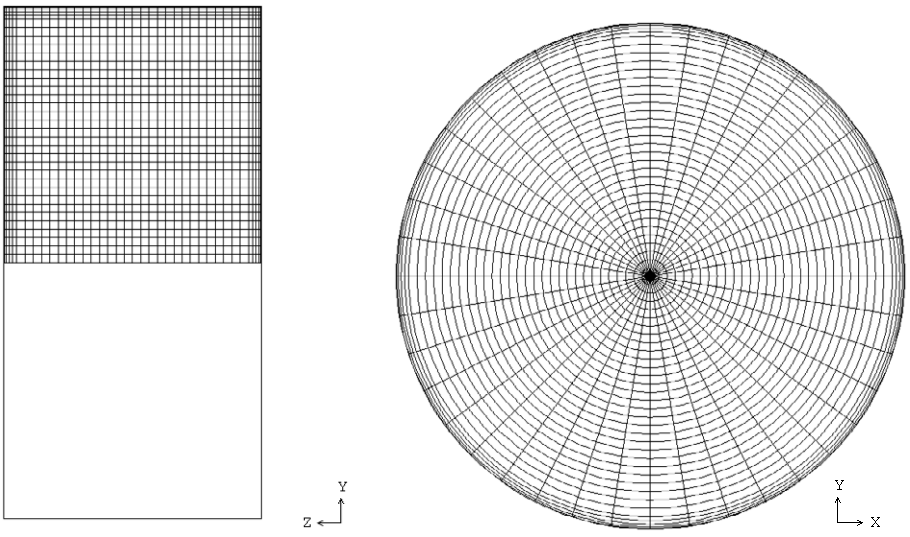

Fig. 2. Cylindrical coordinate meshes for cases of $As = 1.0$.

for $As = 4$ and $40 \times 34 \times 38$ for $As = 1$. Comparing presented results with above grids, the relative errors of resulting oscillatory main frequency are within 1% for $As = 4.0$ with grids $28 \times 20 \times 30$ (case $Ma = 1.65 \times 10^4$) and for $As = 1$ with grids $32 \times 28 \times 30$ (case $Ma = 2.64 \times 10^4$).

3. Validation

The validation of this code for thermocapillary flow computation is checked carefully for both high-Pr and low-Pr flows. For $Pr = 0.01$, $Re = 3500$ ($Re = Ma/Pr$) and $As = 1$, the same stationary non-axisymmetric flow structures ($m = 2$) as that in [13] are obtained. The obtained maximum velocity $U_{\max}$ and velocity component in θ direction, U_θ are 0.0877 and 0.014, respectively, which are comparable with numerical results $U_{\max} = 0.08647$ and $U_\theta = 0.0134$ in [13].

Comparison with the experimental result in [7] is also conducted in the present numerical study. The results are listed in Table 1. The resulting 3-fold symmetrical flow pattern as shown in Fig. 3 is also consistent with experimental report.

4. 3D pulsating oscillatory thermocapillary flow

For small Ma in half-zone, thermocapillary flow is steady and axisymmetrical, but this flow becomes 3D non-axisymmetry with increasing Ma, and this flow mode depends on the Prandtl number Pr. For low-Pr flow, the

Table 1
Comparison of main frequency

ΔT (K)	Ma	Pr	Gr	As	Present result (1/s)	Frank's experimental result (1/s)	
						Way down[a]	Way up[b]
92	28,257	7	240.95	0.73	1.226	1.318	1.357

[a] Way down: decreasing temperature difference to specified ΔT.
[b] Way up: increasing temperature difference to specified ΔT.

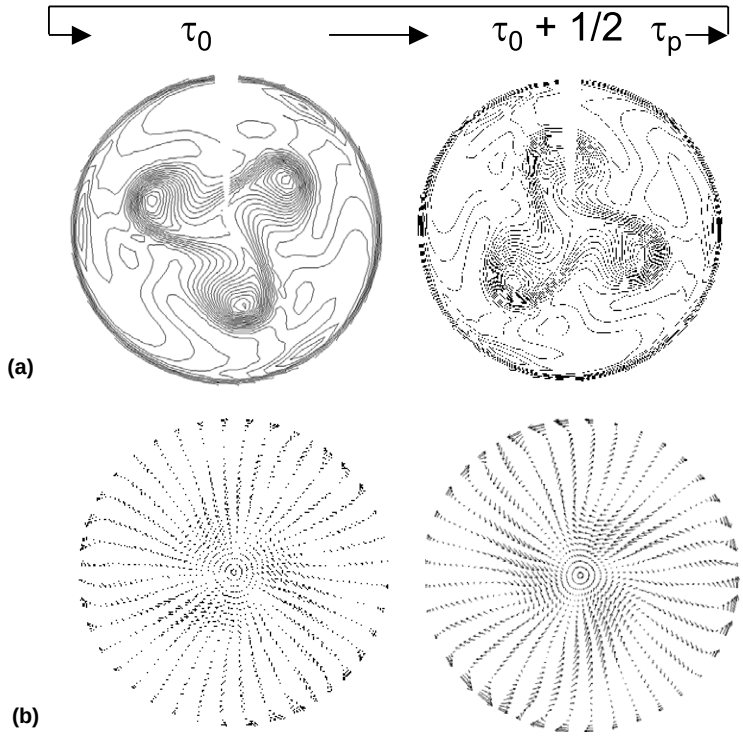

Fig. 3. (a) Temperature contour lines ($\Delta T^* = 0.025$) and (b) projected velocity vector at $z^* = 0.5$, for $Ma = 28{,}257$, $Pr = 7$, $Gr = 240.95$ and $As = 0.73$ within one period.

steady 2D axisymmetric flow becomes stationary 3D non-axisymmetry in the first bifurcation and becomes oscillation in the second bifurcation. In high-Pr flow, steady 2D axisymmetrical flow loses stability to become directly 3D unsteady with increasing Ma. In the present study, 1 cst silicone oil is adopted, and the physical and geometrical conditions are listed in Table 2. For $As = 1$, $Pr = 16.08$, and $Ma = 1.98 \times 10^4$–2.31×10^4, a pulsating temperature and velocity field are observed, and this oscillatory mode prevails throughout the time span of the simulation. By applying fast Fourier transfer (FFT) to temperature or velocity time curve, only one fundamental frequency and its harmonics are found, therefore periodic oscillation is confirmed. As shown in Fig. 4, the cold and hot spots on the free surface are alternated on every half-period, but the positions of cold and hot spots are kept in the oscillatory process. The direction of surface azimuthal velocity is changed after a half-period. And also the 2-fold symmetrical structure can be found in Fig. 4, which corresponds to the so-called azimuthal wave number $m = 2$. The azimuthal velocity is found to grow and decay periodically with time. Fig. 5 shows a temperature contour plot on the free surface within one period. It also demonstrates that the cold and hot spots in azimuthal direction are alternated after a half-period. The standing wave-like oscillatory feature is exhibited in both Figs. 4 and 5. By checking temperature contour plot at the section of $\theta = 0, \pi$ and $\theta = 0.5\pi, 1.5\pi$ in Fig. 6, the phase difference of half-period between $\theta = 0, \pi$ and $\theta = 0.5\pi, 1.5\pi$ can be found easily.

Table 2
Physical and geometrical conditions

Density $\varrho = 818$ kg/m^3
Constant-pressure specific heat $C_p = 1966.48$ J/kg K
Kinematic viscosity $v = 10^{-6}$ m^2/s
Thermal conductivity $k = 0.1$ W/m K
Surface tension $\sigma = 0.04083 - 0.00008404T$ N/m
Gravity $g = 0$ m/s^2
Height of liquid bridge $H = 5$ mm
Temperature difference ΔT and corresponding Marangoni number Ma
$\Delta T = 2.8$ K ($Ma = 2.31 \times 10^4$), $\Delta T = 3.2$ K ($Ma = 2.64 \times 10^4$)

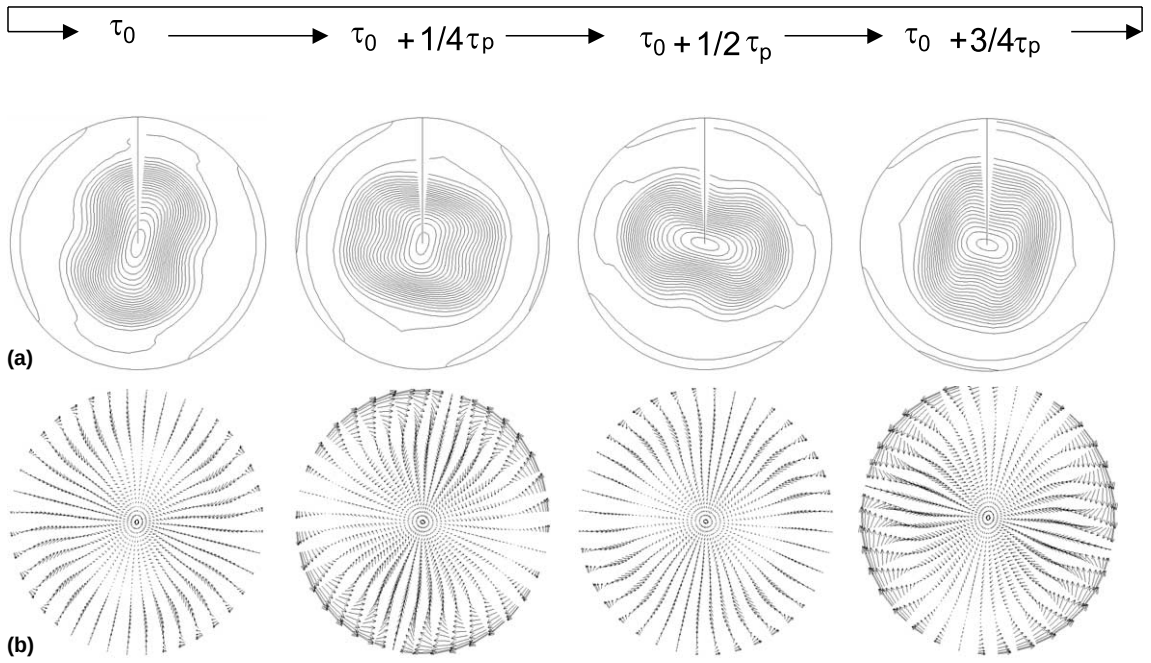

Fig. 4. (a) Dimensionless temperature contour lines ($\Delta T^* = 0.025$) and (b) projected velocity vector at section of $z^* = 0.5$ within one period for $Ma = 2.31 \times 10^4$ and $As = 1$.

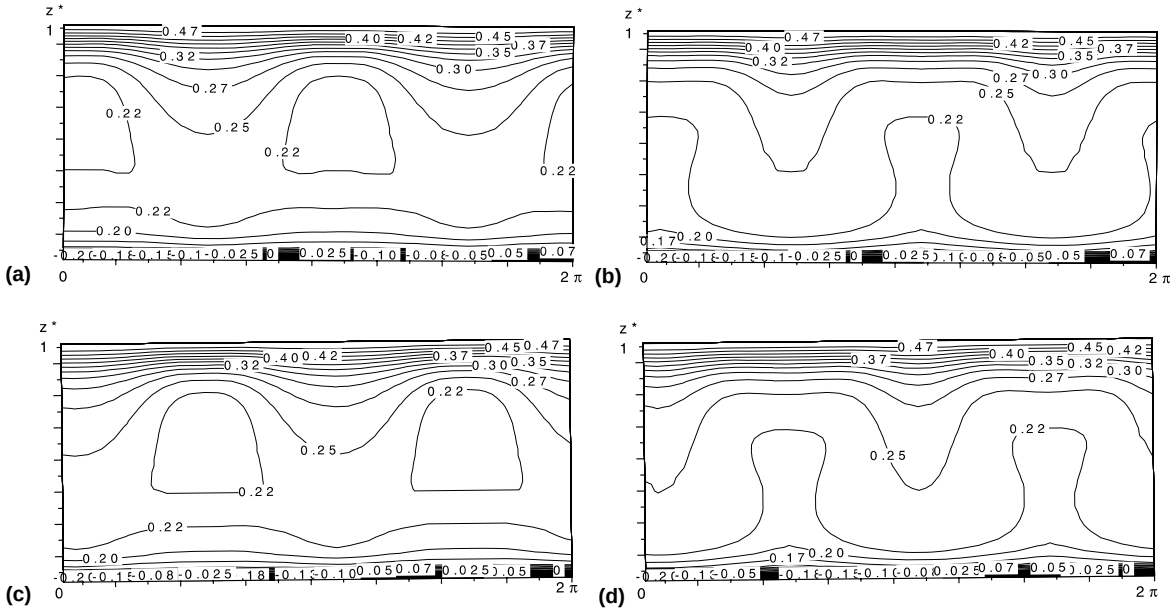

Fig. 5. Contour lines of dimensionless temperature on the free surface at (a) τ_0, (b) $\tau_0 + 1/4\tau_p$, (c) $\tau_0 + 1/2\tau_p$ and (d) $\tau_0 + 3/4\tau_p$ for $Ma = 2.31 \times 10^4$ and $As = 1$.

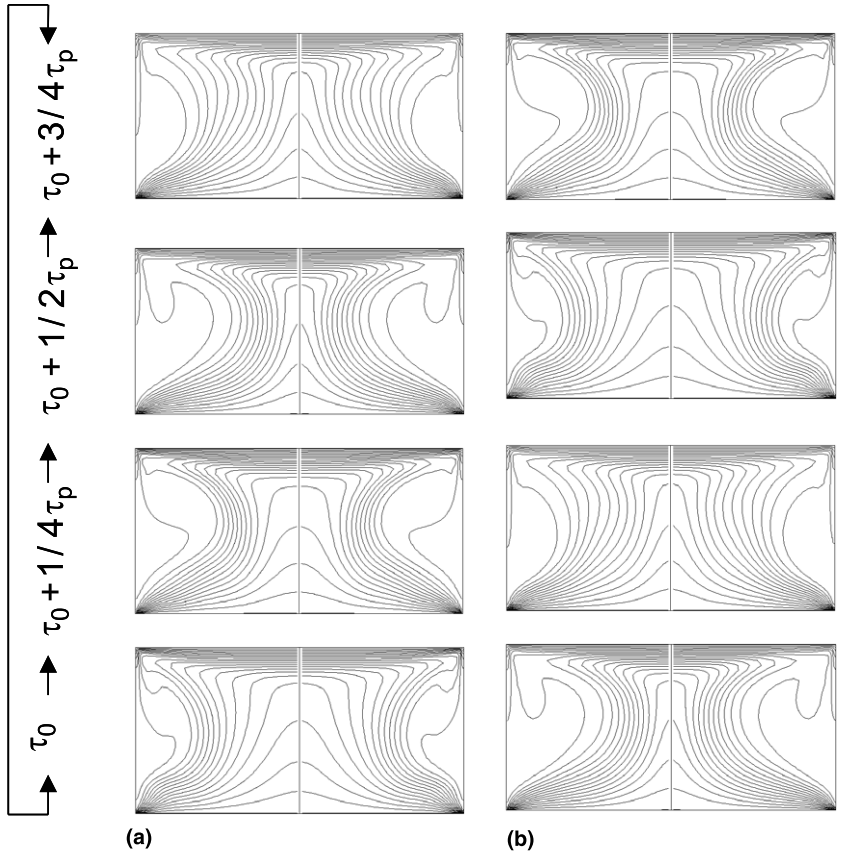

Fig. 6. Dimensionless temperature contour lines ($\Delta T^* = 0.05$) at sections of (a) $\theta = 0, \pi$ and (b) $\theta = 0.5\pi, 1.5\pi$ within one period for $Ma = 2.31 \times 10^4$ and $As = 1$.

5. 3D rotating oscillatory thermocapillary flow

For $As = 1$ and $Ma \geqslant 2.64 \times 10^4$, rather than pulsating oscillation, the rotating oscillatory convection is formed. Fig. 7 shows a temperature contour plot and projected velocity vector at mid-plane, which exhibits a rotating 2-fold symmetrical structure feature. The azimuthal rotating angle is π in one period. Rather than periodic growing and decaying of azimuthal velocity as shown in Fig. 4, the velocity strength is kept in the rotating oscillation as in Fig. 7. Fig. 8 is dimensionless temperature–time curve at points $r = R, z = H/2$ and $\theta = i/20\pi$ $(i = 0, 1, 2, \ldots, 10)$ for both pulsating and rotating oscillatory flow cases. It exhibits that the amplitude of temperature oscillation depends on position alone azimuthal direction for pulsating oscillation as Fig. 8(a). On the contrary, the approximate identical oscillatory amplitude with a phase shift along azimuthal direction is found for rotating oscillatory flow as shown in Fig. 8(b).

For $As = 4$, the azimuthal wave number $m = 1$ is obtained. For $Ma = 1.65 \times 10^4$, the pulsating oscillatory feature is found initially, then it transits to the rotating oscillation automatically. The rotating oscillation becomes stable at about $t^* = 2.4$. (The stable oscillation is defined here such that both the oscillatory amplitude and frequency are kept constant.) The oscillatory main frequency is kept as identical value ($f^* = 131.836$) when pulsating oscillation is replaced by rotating oscillation in this case. For stable oscillatory state, only rotating oscillations are obtained in the present calculated cases for $As = 4$. Fig. 9 indicates a temperature contour plot and projected velocity vector for $Ma = 1.65 \times 10^4$, where the rotating characteristics can be found easily, and the azimuthal rotating angle is 2π in one period.

6. Oscillatory frequencies and *Ma*

By applying FFT to temperature and velocity time curve, the main frequency, which is defined as the frequency with the largest amplitude in FFT spectrum, can be obtained [14], and this main frequency is not found to depend on the position. Fig. 10 exhibits the resulting main frequencies for $As = 1$ and 4. It reveals approximately linear relationship between main frequencies and Ma for $As = 4$ in periodic oscillatory regime. This result is consistent with the experiment in [1] for $As \approx 1.3$–2.0 and also [8] for $As = 1.5$. For $As = 1$, this simple linear relationship does not hold anymore. As shown in Fig. 11, the highest main frequency is at $Ma = 2.31 \times 10^4$, then the main frequency jumps to a low value at larger Ma. With the further increment of Ma, this main frequency keeps a constant, and then increases with the increment of Ma. This frequency feature is similar to the experimental report in [6] for $As \approx 1$, and also to the reports in [8] for $As \approx 0.83$. Based on the present simulations, the phenomenon of lower main frequency for higher Ma is speculated to be caused by the change from pulsating to rotating oscillatory modes. In Fig 11, the oscillations

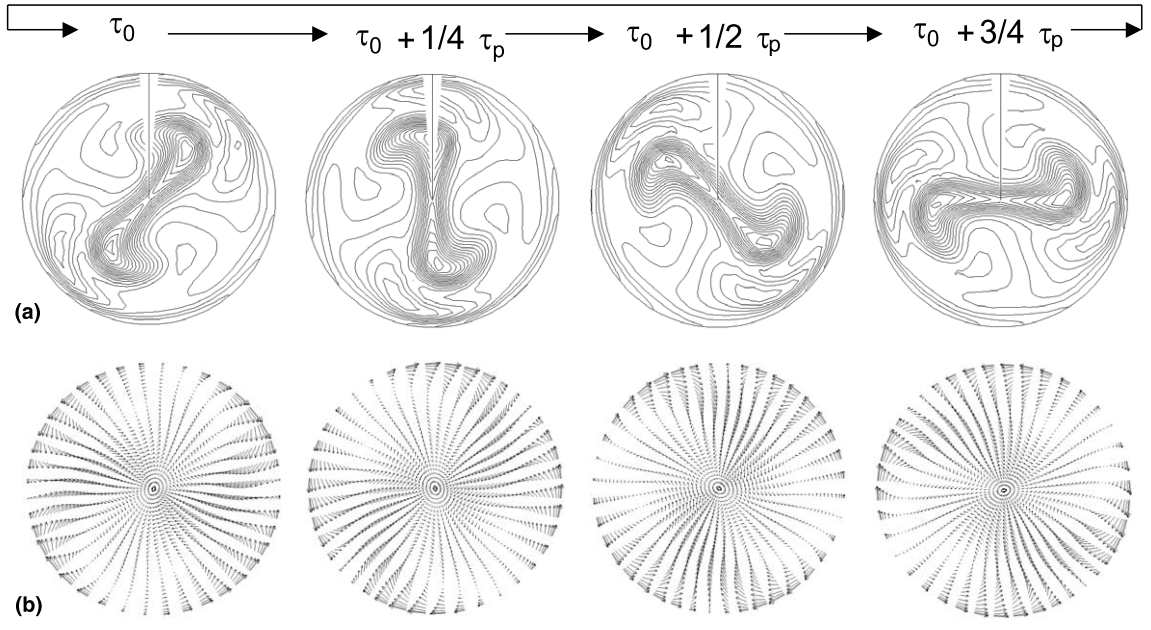

Fig. 7. (a) Dimensionless temperature contour lines ($\Delta T^* = 0.025$) and (b) projected velocity vector at section of $z^* = 0.5$ within one period for $Ma = 2.64 \times 10^4$ and $As = 1$.

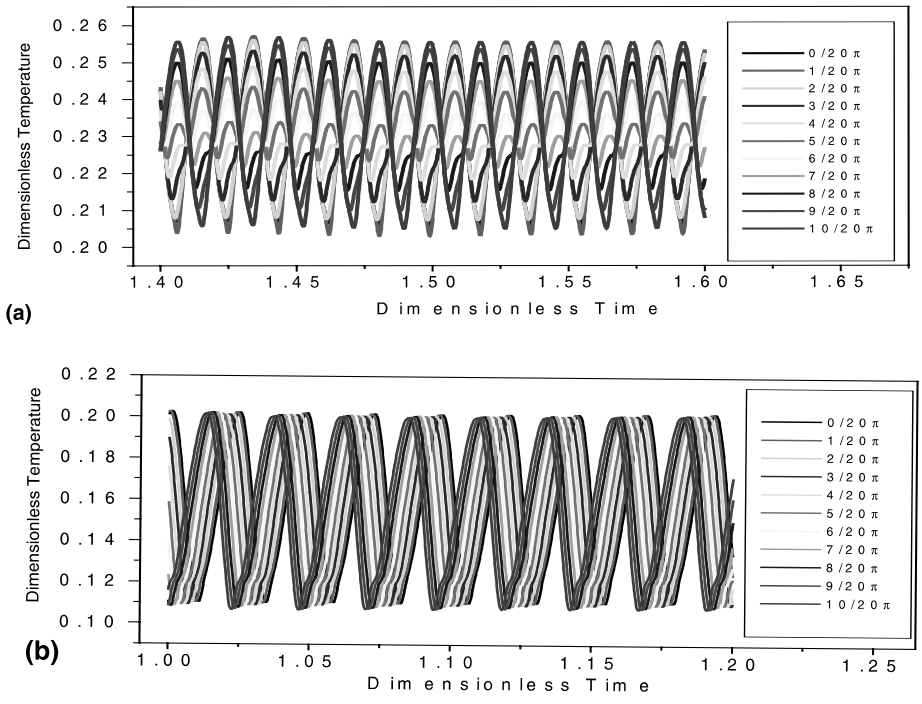

Fig. 8. Dimensionless temperature–time curves at points $r = R$, $z = H/2$ and $\theta = i/20\pi$ ($i = 0, 1, 2, \ldots, 10$) for $Pr = 16.0849, As = 1.0$ (a) $Ma = 2.31 \times 10^4$ and (b) $Ma = 2.64 \times 10^4$.

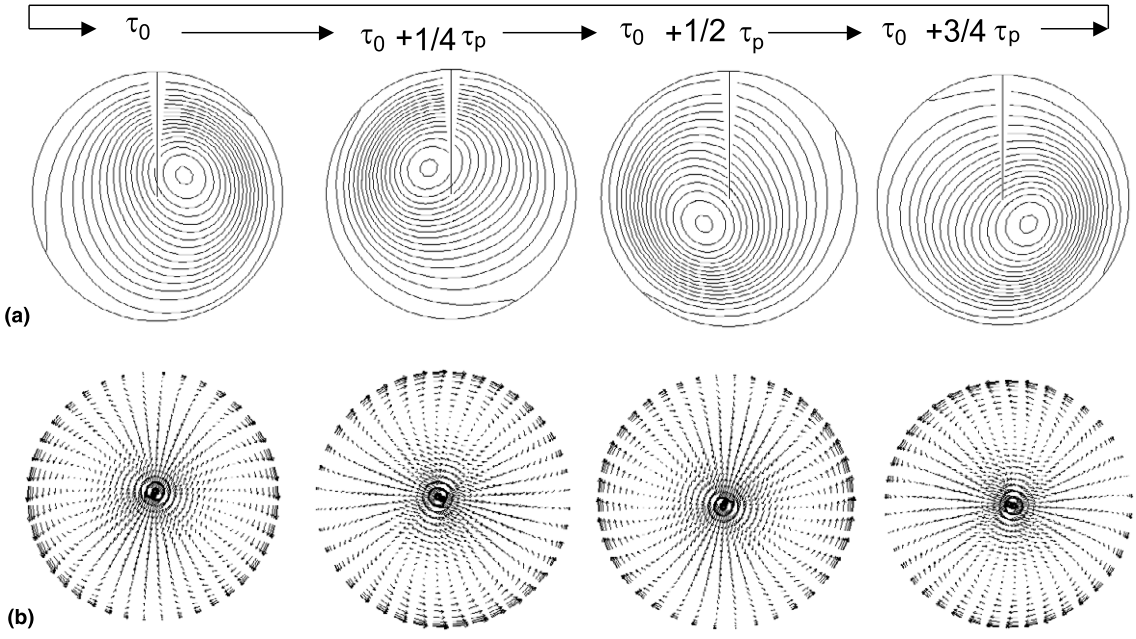

Fig. 9. (a) Dimensionless temperature contour lines ($\Delta T^* = 0.025$) and (b) projected velocity vector at section of $z^* = 0.5$ within one period for $Ma = 1.65 \times 10^4$ and $As = 4$.

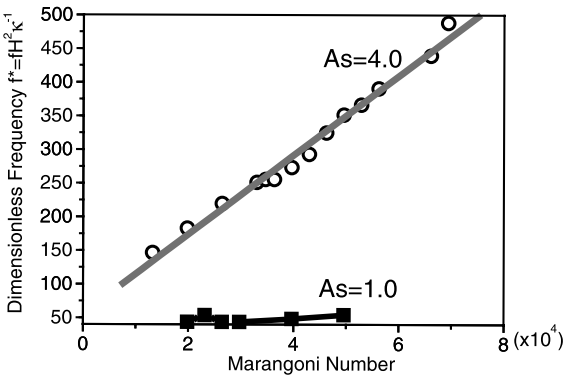

Fig. 10. Relationship between Ma and dimensionless main frequency f^* for $As = 4$ and 1, $Pr = 16.08$ in periodic oscillatory regime.

for $Ma = 1.98 \times 10^4$ and 2.31×10^4 are pulsating mode, and the oscillation at points with $Ma \geqslant 2.64 \times 10^4$ in Fig 11 is rotating mode. In fact, pulsating oscillation is also found initially for $As = 1$ and $Ma = 2.64 \times 10^4$, then it becomes rotating oscillation automatically in the evolution of flow structure. In this case, the oscillatory main frequency is $f^* = 58.594$ in initial pulsating oscillatory regime, and then it decreases to $f^* = 43.945$ when the pulsating oscillatory mode is replaced by rotating oscillatory mode. In the most recent reference [14], amplitude equations of hydrothermal waves for the weakly non-linear behavior were solved, the required parameters in amplitude equations were fitted from data based on 3D numerical simulation. They reported that finite amplitude azimuthally standing wave (pulsating oscillation) decays to traveling waves (rotating oscillation) under conditions of $Pr = 4$, $As = 1$ and $Gr = 0$, and close to the critical Re, the former may persist for long time. To confirm their conclusion, a solution of oscillatory convection for $As = 1$ and $Ma = 2.64 \times 10^4$ is taken as initial condition for the case of $As = 1$ and $Ma = 2.32 \times 10^4$, instead of retaining rotating oscillatory mode, the convection returns to pulsating oscillatory mode within thermal diffusion time $t^* < 0.2$, and this mode prevails within the time span of simulation ($t^* = 2.0$). This result implies the complexity of the evolution of oscillatory mode, and it neither supports nor denies Leypoldt's conclusion under the present conditions: $Pr = 16.8$, $Gr = 0$ and $As = 1$. Because this 3D simulation is time consuming, the available CPU time does not allow a further confirmation in a direct 3D simulation.

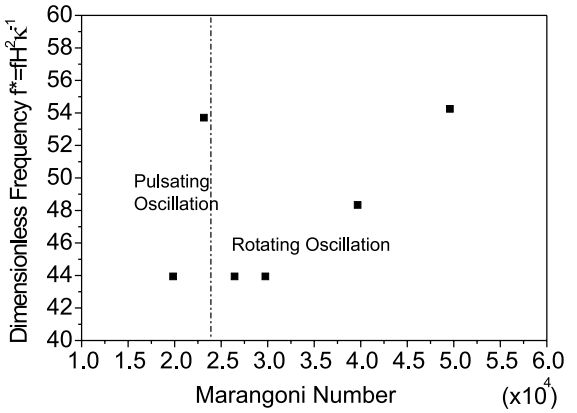

Fig. 11. Relationship between Ma and dimensionless main frequency f^* for $As = 1$ and $Pr = 16.08$.

7. Conclusion

Three-dimensional oscillatory thermocapillary flow in half-zone liquid bridge is investigated by means of FVM. For $As = 1$, 2-fold symmetrical structure is obtained in mid-plane, and there are two types of oscillatory modes: pulsating and rotating modes. For Ma close to the onset of oscillation, the pulsating oscillatory mode is observed throughout the time span of simulation. With further increasing Ma, the pulsating oscillatory mode is replaced by rotating oscillation. The f^*–Ma plot demonstrates a frequency jump at $Ma = 2.31 \times 10^4$. Based on the present simulations, the observed phenomenon of higher main frequency with lower Ma is speculated to be caused by the change of oscillatory modes: from pulsating to rotating oscillatory modes. For $As = 4$, azimuthal wave number m is 1, only rotating oscillation is found to be stable in the present calculated cases and dimensionless main frequencies are approximately proportional to Ma in periodic oscillatory regime.

Acknowledgements

This work is financially supported by Ishikawajima-Harima Heavy Industries (IHI). The authors are thankful to the crew of Information Science Group of Institute for Materials Research for the continuous support of the computer environment.

References

[1] D. Schwabe, A. Scharmann, F. Preisser, R. Oeder, Experiments on surface tension driven flow in floating zone melting, J. Cryst. Growth 43 (1978) 305–312.
[2] D. Schwabe, A. Scharmann, Some evidence for the existence and magnitude of a critical Marangoni number for the onset of oscillatory flow in crystal growth melts, J. Cryst. Growth 46 (1979) 125–131.
[3] D. Schwabe, Marangoni effects in crystal growth melts, Physico-Chem. Hydrodyn. 2 (1981) 263–281.

[4] F. Preisser, D. Schwabe, A. Scharmann, Steady and oscillatory thermocapillary convection in liquid columns with free cylindrical surface, J. Fluid Mech. 126 (1983) 545–567.
[5] D. Schwabe, Surface-tension-driven flow in crystal growth melts, in: H.C. Freyhardt (Ed.), Crystals, vol. 11, Springer, Berlin, Heidelberg, 1988, pp. 75–112.
[6] R. Velten, D. Schwabe, A. Scharmann, The periodic instability of thermocapillary convection in liquid columns with free cylindrical surface, Phys. Fluids A3 (1991) 267–279.
[7] S. Frank, D. Schwabe, Temporal and spatial elements of thermocapillary convection in zones, Exp. Fluids 23 (1997) 234–251.
[8] D. Schwabe, S. Frank, Experiments on the transition to chaotic thermocapillary flow in floating zones under microgravity, Adv. Space Res. 24 (1999) 1391–1396.
[9] S. Nakamura, T. Hibiya, K. Kakimoto, N. Imaishi, S. Nishizawa, A. Hirata, K. Mukai, S. Yoda, T.S. Morita, Temperature fluctuations of the Marangoni flow in a liquid bridge of molten silicon under microgravity on board the TR-IA-4 rocket, J. Cryst. Growth 186 (1998) 85–94.
[10] R. Savino, R. Monti, Oscillatory Marangoni convection in cylindrical liquid bridges, Phys. Fluids 8 (1996) 2906–2922.
[11] S. Yasuhiro, T. Sato, N. Imaishi, Three-dimensional oscillatory Marangoni flow in half-zone of $Pr = 1.02$ fluid, Microgravity Sci. Techn. X/3 (1997) 144–153.
[12] J. Leypoldt, H.C. Kuhlmann, H.J. Rath, Three-dimensional numerical simulation of thermocapillary flows in cylindrical liquid bridges, J. Fluid Mech. 414 (2000) 285–314.
[13] M. Levenstam, G. Amberg, Hydrodynamic instabilities of thermocapillary flow in a half-zone, J. Fluid Mech. 297 (1995) 357–372.
[14] Z. Zeng, H. Mizuseki, K. Higashino, Y. Kawazoe, Direct numerical simulation of oscillatory Marangoni convection in cylindrical liquid bridges, J. Cryst. Growth 204 (1999) 395–404.